Deterministic Von Mises–Fisher Sampling on the Sphere Using Fibonacci Lattices

Daniel Frisch and Uwe D. Hanebeck
Intelligent Sensor-Actuator-Systems Laboratory (ISAS)
Karlsruhe Institute of Technology (KIT)
Karlsruhe, Germany
{daniel.frisch, uwe.hanebeck}@ieee.org.

***Abstract*—We propose a von Mises–Fisher sampling scheme using Fibonacci lattices to generate high-quality deterministic samples on the sphere. Key idea is an orthogonal inverse transform to map uniform low-discrepancy or quasi-random samples, ideally from Fibonacci lattices, to the sphere. The proposed new sampling method can be applied in assumed density Riemannian particle filters and controllers. Compared to random sampling, it produces well-separated, locally homogeneous samples, yielding superior convergence in numerical applications. The advantage over UKF-like sampling schemes is the free choice of the number of samples.**

***Index Terms*—von Mises–Fisher density, Fisher density, low-discrepancy sequence, Fibonacci lattice, Sobol sequence, deterministic sampling, non-Euclidean, Riemannian, cubature, particle filter**

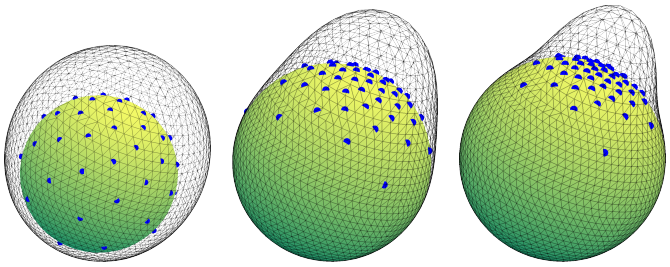

(a) $\kappa = 1$ (b) $\kappa = 5$ (c) $\kappa = 10$

Fig. 1: Sets of 50 von Mises–Fisher (or Fisher) samples with different concentration parameters κ, produced by our proposed method.

I. Introduction

Sampling from a given probability density function is a central building block in many applications. The most prominent application is cubature, i.e., approximating numerical integration in higher dimensions. Cubature is a building block in many applications, such as sensor data fusion, prediction, state estimation, control, Bayesian optimization, and finance. As opposed to the often-used mutually independent, identically distributed (iid) random samples, deterministic samples provide better coverage of the space and convergence of the integral [1]. In global optimization, a set of initial guesses has to be distributed evenly in high-dimensional spaces. Deterministic samples cover the space more efficiently than random samples [2]. Also, the apparently simple placement of sensors [3], LED lights, boreholes, or plant seeds can be viewed as a sampling problem. An elegant solution is seen in many flower heads: the Fibonacci grid, yielding a conspicuous spiral pattern, combines superior packing efficiency with flexibility during growth [4].

The above examples are usually considered in Euclidean spaces. However, their analysis on Riemannian manifolds becomes more and more important. In modern wireless communications, the angle of arrival (AoA) distribution is modeled with spherical densities to facilitate highly efficient data transmission using multiple inputs multiple outputs (MIMO) techniques [5]. Wind directions in weather simulations [6] can only be truthfully represented via a vector field with vectors from Riemannian manifolds. Robotic design, kinematics, and path planning require optimization, state estimation, and control on (hyper)spheres and (hyper)tori [7], [8]. Aircraft require sophisticated balancing control. Their state is best represented via quaternions that, in turn, require a hyperhemispherical manifold [9].

Computations are often performed on linearized Euclidean tangent spaces of the underlying Riemannian manifolds. This works well if uncertainties are small. However, with greater uncertainty, performing the calculations directly on the nonlinear manifold becomes increasingly important. If a significant part of the probability mass protrudes beyond periodicity limits, the result will otherwise be distorted even with an optimally selected linearization point. Drones and robots have become smaller and more versatile. Therefore, the predictions of the internal motion models (that must reflect the physical capabilities) become more uncertain: a small drone can make sudden changes in direction and speed that a passenger aircraft would not be physically capable of. Weather simulations get more fine-grained, and the individual forecasts, limited to smaller areas, are more unstable. Products are pushing into the mass market, equipped with more but cheaper sensors that provide unreliable measurement data.

In summary, processing *uncertain* sensor data on *nonlinear manifolds* becomes increasingly essential. This work addresses this challenge with a novel sampling algorithm for the spherical von Mises–Fisher (or Fisher) distribution.

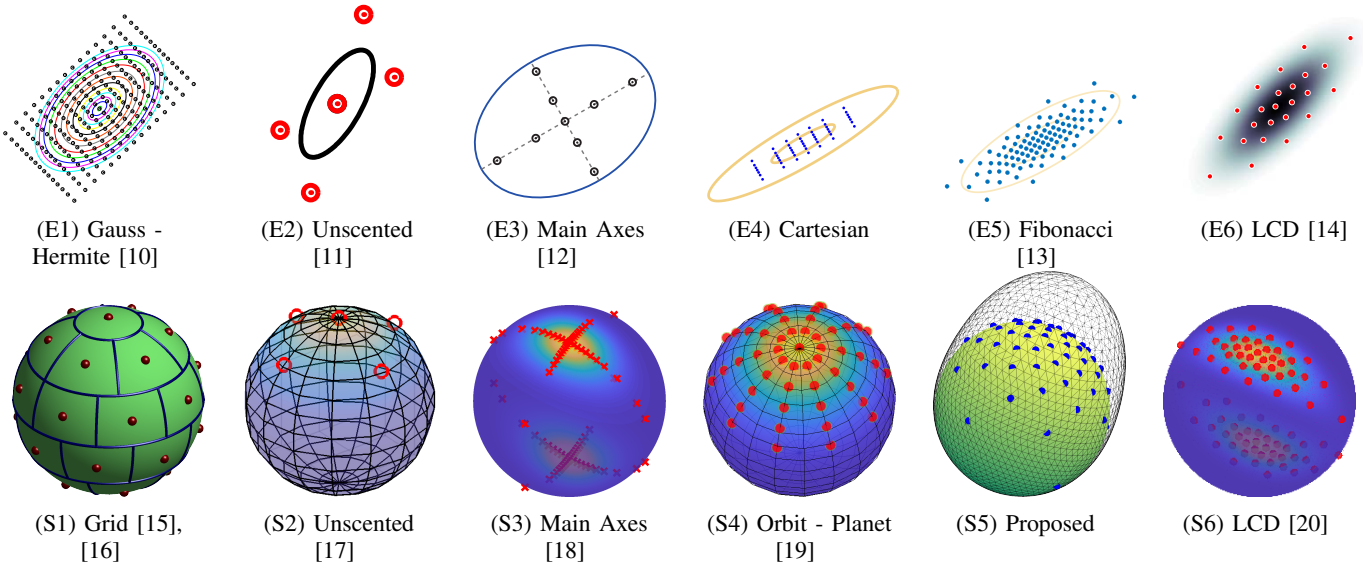

Fig. 2: Different types of Gaussian sampling in Euclidean space (top, E1 … E6) and von Mises–Fisher and Bingham sampling on the spherical domain (bottom, S1 … S6). Figures are captured from the stated references. First column (E1, S1) shows uniform-grid-based filters with individually weighted samples, second column (E2, S2) moment matching, other columns equally weighted samples. Note that LCD samples (E6, S6) are much slower to compute than all others. We propose low-discrepancy sampling with Fibonacci lattices on the sphere (S5), as it produces high-quality results *and* is fast.

The most widely used deterministic sampling method is based on moment matching. Sample locations can be computed, for example, by matching mean and covariance in Euclidean domains [21] (see Fig. 2E2), and trigonometric moments on (hyper)spherical manifolds [17] (see Fig. 2S2). The major limitation here is that the number of samples is fixed and cannot be adapted to the complexity of the problem. Furthermore, how many and which moments should be considered is usually unclear. The number of samples may be increased by placing more samples on the main axes [12] (see Fig. 2E3), and analogously on (hyper)spheres [18], [22] (see Fig. 2S3). However, this approach still misses the areas apart from the principal axes, so the probability mass present there is not adequately represented. This can be improved by using an "orbit-planet" sample arrangement [23], [19] (see Fig. 2S4). It can be seen as mapping a regular Cartesian grid such as the one in Fig. 3b to the sphere. However, this leads to the "concatenation" of samples to circular rings near the pole and lines near the equator, yielding bad coverage of the space locally. We propose using a low-discrepancy reference grid instead of the Cartesian grid to overcome this coverage problem (see Fig. 2S5). We already proposed a similar sampling scheme for the Gaussian density [13], [24] (see Fig. 2E5).

The Localized Cumulative Distribution (LCD) can also be used to produce arbitrary numbers of deterministic samples in Euclidean domains [25] (see Fig. 2E6), as well as Riemannian domains [26], [20] (see Fig. 2S6). These samples provide very good homogeneous state space coverage according to the desired density, arguably the best. However, one must solve a nonlinear optimization problem to obtain the samples, which might be too expensive for real-time applications.

In summary, existing deterministic sampling methods are either inflexible or computationally expensive. Therefore, we propose a sampling method that is fast and cheap to compute and provides flexibility in the number of produced samples.

Our proposed deterministic sampling method is heavily based on low-discrepancy point sets. Compared to independent uniformly distributed samples (see Fig. 3a), low-discrepancy point sets cover the space locally homogeneously (see Figs. 3c and 3d). Specifically, low discrepancy means that all possible axes-aligned rectangles inside the unit square $[0, 1]^2$ contain a number of samples that is approximately proportional to their volume. And other than the regular axis-aligned square grid (see Fig. 3b), every point has unique x and y coordinates, respectively (see Fig. 3c). This ensures that the function into which these points are inserted is evaluated with genuinely different coordinates for every single sample. Low-discrepancy point sets retain their local homogeneity if anisotropically scaled along the coordinate axes [24].

We exploit this transformability to obtain spherical von Mises–Fisher samples via a suitable two-dimensional inverse transform. The von Mises–Fisher density on the $\mathbb{S}^2$ sphere is also called Fisher density since it was first studied in detail by Sir Ronald Fisher [27]. After the uniform density, it is the most basic distribution on the sphere [28, pp. 167–173]. Considering the limiting case of concentrated densities, it is identical to the isotropic wrapped normal density [28, pp. 172–173], [26, Sec. 6]. The (von Mises–)Fisher density has applications with direction-of-arrival measurements [29], e.g., object tracking

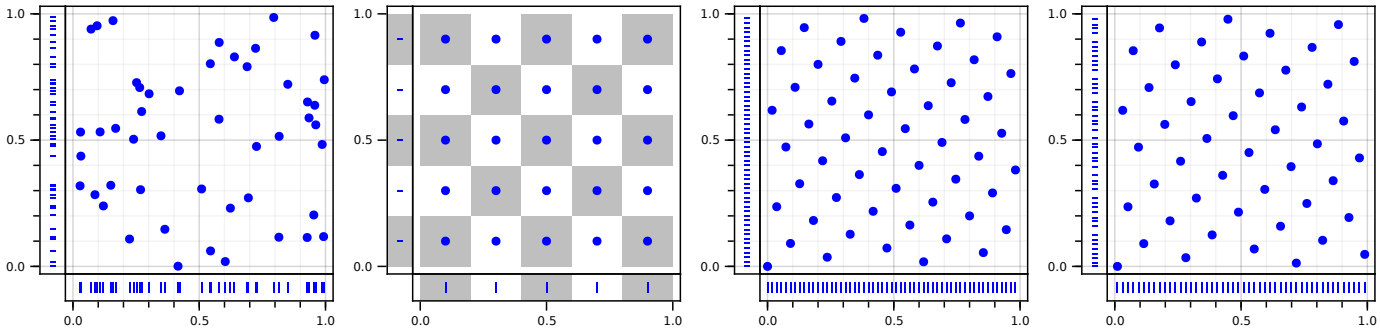

(a) Random. (b) Cartesian. (c) Fibonacci–rank-1 lattice. (d) Fibonacci–Kronecker lattice.

Fig. 3: Uniform samples in the two-dimensional unit square $\underline{x} \in [0,1]^2$.

using an omnidirectional camera [30], and in white matter fiber tracking using diffusion tensor magnetic resonance imaging (DT-MRI) of the brain [31].

II. Uniform Reference Point Sets

This section describes suitable uniform reference point sets that will later be transformed to the von Mises–Fisher density. We focus on low-discrepancy point sets rather than random samples as they provide superior convergence in numerical integration applications [1, p. 176].

A. Equidistant Point Sets, for $D = 1$

In the scalar case, the best choice is simply the equidistant point set

$$x_i = i \cdot \frac{1}{L} \quad , \qquad i \in \{0, 1, \ldots, L-1\} \quad . \tag{1}$$

This can be seen as a rank-1 lattice with generator $\frac{1}{L}$. Sometimes, it is beneficial to use the centered version

$$x_i = \frac{2i-1}{2L} \quad , \qquad i \in \{1, \ldots, L\} \quad , \tag{2}$$

where no sample is exactly zero or one.

B. Golden Sequence, for $D = 1$

If the point set should be extensible while keeping the previous samples in place, the golden sequence is a good choice

$$x_i = i \cdot \frac{1}{\Phi} \mod 1 \quad , \qquad i \in \{0, 1, \ldots, L-1\} \quad , \tag{3}$$

with

$$\frac{1}{\Phi} = \frac{\sqrt{5}-1}{2} = 0.618\ldots \quad . \tag{4}$$

This can be seen as a Kronecker sequence with generator $\frac{1}{\Phi}$. Centering can be performed here by simply counting i in $\{1, \ldots, L\}$ instead of in $\{0, \ldots, L-1\}$.

C. Fibonacci–Rank-1 Lattice, for $D = 2$

The best possible [32] low-discrepancy point set in the periodic unit square $[0,1)^2$ is the Fibonacci lattice

$$\underline{x}_i = i \cdot \begin{bmatrix} \frac{1}{F_{k+1}} \\ \frac{F_k}{F_{k+1}} \end{bmatrix} \mod 1 \quad , \qquad i \in \{0, 1, \ldots, F_{k+1}-1\} \quad , \tag{5}$$

where F_k is the k-th Fibonacci number [1, Ex. 2.8], $k \in \mathbb{N}$. This is a two-dimensional rank-1 lattice. The point set is periodic along both axes and can be projected onto a torus. Note that the total number L of lattice points $\underline{x}_i$ must be a Fibonacci number, $L = F_{k+1}$ (see Fig. 3c). A centered variant would be

$$\underline{x}_i = i \cdot \begin{bmatrix} \frac{1}{F_{k+1}} \\ \frac{F_k}{F_{k+1}} \end{bmatrix} + \frac{1}{2F_{k+1}} \mod 1 \quad , \qquad i \in \{0, 1, \ldots, F_{k+1}-1\} \quad . \tag{6}$$

D. Fibonacci–Kronecker Lattice, for $D = 2$

A somewhat similar point set is also well known [33, Eq. 3]. It is a Kronecker lattice that again generates points $\underline{x}_i$ in the unit square $[0,1)^2$

$$\underline{x}_i = i \cdot \begin{bmatrix} \frac{1}{L} \\ \frac{1}{\Phi} \end{bmatrix} \mod 1 \quad , \qquad i \in \{0, 1, \ldots, L-1\} \quad . \tag{7}$$

It can be seen as combining the one-dimensional equidistant point set (1) and the golden sequence (3). In contrast to (5), the total number of points L is not restricted to Fibonacci numbers here. One marginal (the one whose generator is $\frac{1}{L}$) is equidistant, and the other is not (see Fig. 3d). The point set is periodic only along one dimension (the one whose generator is $\frac{1}{\Phi}$) and should, therefore, not be projected onto a torus but is suitable for projection onto the sphere and the cylinder. A centered variant is given as

$$\underline{x}_i = \begin{bmatrix} \frac{2i-1}{2L} \\ \frac{i}{\Phi} \end{bmatrix} \mod 1 \quad , \qquad i \in \{1, \ldots, L\} \quad . \tag{8}$$

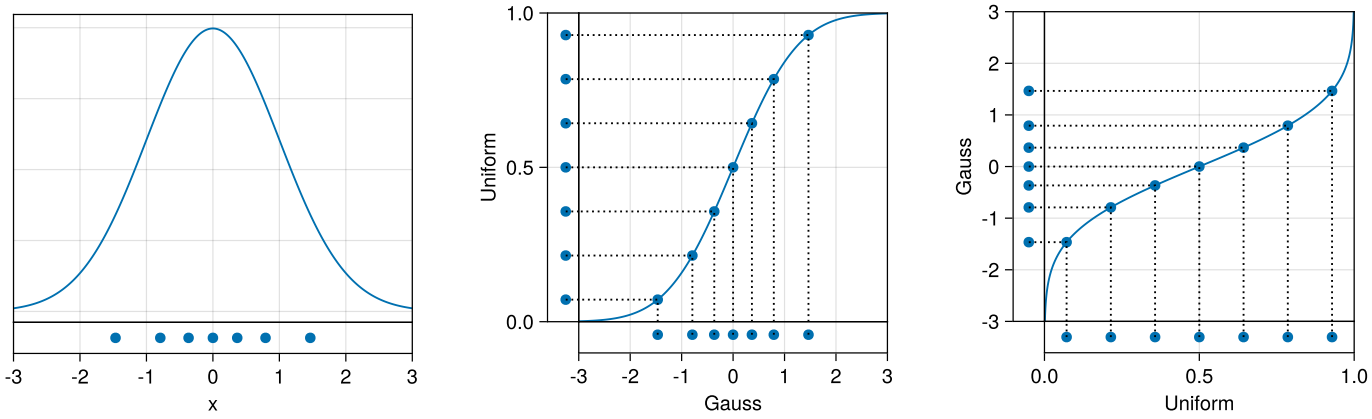

(a) PDF (12) $f_{\mathcal{N}}(x)$ (b) CDF (13) $F_{\mathcal{N}}(x)$ (c) Quantile function (14) $Q_{\mathcal{N}}(p)$

Fig. 4: Transforming uniform deterministic samples to standard normal via inverse transform sampling. Uniform samples can be transformed through the inverse of the CDF, yielding Gaussian samples (b). Equivalently, uniform samples can also be transformed through the quantile function, again yielding Gaussian samples (c).

E. Random Samples

While we strongly recommend using the Fibonacci–rank-1 lattice and the Fibonacci–Kronecker lattice as reference point sets, of course, independent random samples could also be used, resulting in mutually independent von Mises–Fisher samples. An equivalent random von Mises–Fisher sampling approach has been proposed in [34]. According to the Central Limit Theorem, the Monte Carlo convergence resulting from random samples will be only $1/\sqrt{L}$. Loosely speaking, Monte Carlo estimates based on random samples have a larger variance than quasi-Monte Carlo estimates with the proposed quasi-random or low-discrepancy Fibonacci lattices. However, the expected variance of the estimate is more precisely known for random samples due to the Central Limit Theorem. An error estimate for our proposed method could still be obtained via random shifting [1, pp. 155–157].

III. Transformations

To obtain non-uniform samples, like samples from the von Mises–Fisher density, the low-discrepancy sequences have to be transformed accordingly.

A. Univariate Densities, $D = 1$

Transformations are particularly simple in the univariate case. Suppose we want to obtain deterministic samples of a probability density $f(x)$ with $x \in \mathbb{R}$. First, we calculate its cumulative distribution function

$$F(x) = \int_{-\infty}^{x} f(u)\,\mathrm{d}u \ . \tag{9}$$

The desired non-uniform samples $x_i^f \sim f(x)$ are now computed by propagating uniform samples $x_i^{\mathrm{u}} \in [0, 1]$ through the quantile function $Q(p)$, which is the inverse of the cumulative distribution [35, Theorem 8]

$$x_i^f = Q(x_i^{\mathrm{u}}) \ , \tag{10}$$

$$Q(p) = F^{-1}(p) \ . \tag{11}$$

Example – Univariate Standard Normal Density: For the univariate standard normal desity $f_{\mathcal{N}}(x)$

$$f_{\mathcal{N}}(x) = \frac{1}{\sqrt{2\pi}\sigma} \cdot \exp\left\{-\frac{1}{2}\left(\frac{x}{\sigma}\right)^2\right\} \ , \tag{12}$$

we can write its cumulative distribution $F_{\mathcal{N}}(x)$ as

$$F_{\mathcal{N}}(x) = \frac{1}{2} \cdot \left(1 + \mathrm{erf}\left(\frac{x}{\sqrt{2}}\right)\right) \tag{13}$$

and its quantile function $Q_{\mathcal{N}}(p)$

$$Q_{\mathcal{N}}(p) = \sqrt{2} \cdot \mathrm{erf}^{-1}(2 \cdot p - 1) \tag{14}$$

in closed form using the Gaussian error function $\mathrm{erf}(\cdot)$ and its inverse (see Fig. 4). The quantile function $Q_{\mathcal{N}}(p)$ of the standard normal density is also called the probit function. To obtain Gaussian samples, we can take uniform samples x_i^{u}, e.g., centered equidistant samples (2), regard them as quantiles, and transform them via the probit function $Q_{\mathcal{N}}(\cdot)$ to Gaussian samples $x_i^{\mathcal{N}}$

$$x_i^{\mathcal{N}} = Q_{\mathcal{N}}(x_i^{\mathrm{u}}) \tag{15}$$

$$= \sqrt{2} \cdot \mathrm{erf}^{-1}\left(\frac{2\,i - 1}{L} - 1\right) \tag{16}$$

(see Fig. 4c).

B. Multivariate Densities, $D > 1$

For *multivariate* densities, sampling is simplified if they are separable. In that case, they can be written as the product of their marginals, i.e., the densities of independent univariate random variables that correspond to the coordinate axes

$$f(x, y, z, \ldots) = f_x(x) \cdot f_y(y) \cdot f_z(z) \cdots \ . \tag{17}$$

Then, each coordinate can be treated individually according to (10), respectively. Otherwise, we have to first look for a suitable orthogonal coordinate system such that the density

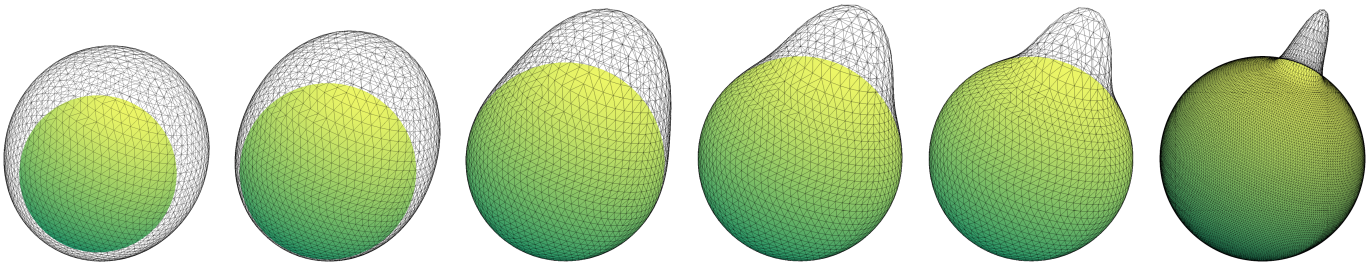

(a) $\kappa = 1$ (b) $\kappa = 2$ (c) $\kappa = 5$ (d) $\kappa = 10$ (e) $\kappa = 20$ (f) $\kappa = 100$

Fig. 5: Effect of the parameter κ on the von Mises–Fisher density function.

is separable into those coordinates. For example, for multivariate Gaussians, such a mapping involves the eigenvalue decomposition of the covariance matrix [13]. Others have instead used the Cholesky decomposition [36], [37]. The Cholesky-based inverse transform is, however, not orthogonal and deteriorates the homogeneity of the samples (see [24, Fig. 8]). The possibility of mapping two-dimensional low-discrepancy grids to the sphere $\mathbb{S}^2$ and the cylinder $\mathbb{S}^1 \times \mathbb{R}$ has been noted before [38], but the opportunity to explicitly approximate non-uniform spherical density functions like the von Mises–Fisher density has not been explored yet.

IV. Von Mises–Fisher Density on $\mathbb{S}^2$

We describe the workflow of finding an orthogonal mapping that, given uniform samples, produces the von Mises–Fisher distribution

$$f(\underline{x}) = \frac{\kappa}{2\pi\left(e^{\kappa} - e^{-\kappa}\right)} \cdot \exp\left\{\kappa \cdot \underline{\mu}^{\top}\underline{x}\right\} \quad , \tag{18}$$

$$\underline{\mu}, \underline{x} \in \mathbb{S}^2 \subset \mathbb{R}^3 \tag{19}$$

on the $\mathbb{S}^2$ sphere. Parameter $\underline{\mu}$ defines the mode of the density, and parameter κ the directional uncertainty. See Fig. 5 for a visualization of von Mises–Fisher density functions $f(\underline{x})$ with various choices of κ. First, we settle on the spherical coordinate system $[\theta, \varphi]^{\top}$ with coordinate transformation ζ

$$\zeta \colon \mathbb{S}^2_{\mathrm{SC}} \to \mathbb{S}^2 \subset \mathbb{R}^3 \tag{20}$$

$$\zeta \colon \begin{bmatrix}\theta \\ \varphi\end{bmatrix} \to \begin{bmatrix}\cos(\theta) \\ \sin(\theta)\cos(\varphi) \\ \sin(\theta)\sin(\varphi)\end{bmatrix} \quad , \tag{21}$$

where $\mathbb{S}^2_{\mathrm{SC}}$

$$\mathbb{S}^2_{\mathrm{SC}} = [0, \pi] \times [0, 2\pi]$$

is the domain of the spherical coordinates $[\theta, \varphi]^{\top}$. This coordinate transform serves as our skeleton grid. Because it is orthogonal [39], the resulting transformed low-discrepancy points retain their local homogeneity [40]. Without loss of generality, we consider $\underline{\mu} = \underline{e}_1 = \begin{bmatrix}1 & 0 & 0\end{bmatrix}^{\top}$ (the final cloud of samples can be shifted on the sphere later) and obtain

$$f(\theta, \varphi) = \frac{\kappa}{2\pi\left(e^{\kappa} - e^{-\kappa}\right)} \cdot \exp\{\kappa \cdot \cos(\theta)\} \quad , \tag{22}$$

and with the surface area element of the $\mathbb{S}^2$ sphere in spherical coordinates,

$$\mathrm{d}_{\mathbb{S}^2} A = \sin(\theta)\,\mathrm{d}\theta\,\mathrm{d}\varphi \quad , \tag{23}$$

we can compute the cumulative distribution $F(\theta, \varphi)$

$$F(\theta, \varphi) \propto \int_0^{\varphi}\int_0^{\theta} \exp\Big\{\kappa \cdot \cos(\tilde{\theta})\Big\} \cdot \sin(\tilde{\theta})\,\mathrm{d}\tilde{\theta}\,\mathrm{d}\tilde{\varphi} \tag{24}$$

$$\propto \left(\exp\{\kappa\} - \exp\{\kappa \cdot \cos(\theta)\}\right) \cdot \varphi \tag{25}$$

in spherical coordinates $[\theta, \varphi]^{\top} \in \mathbb{S}^2_{\mathrm{SC}}$. Thus, we obtain a separable cumulative distribution function

$$F(\theta, \varphi) = F_1(\theta) \cdot F_2(\varphi) \tag{26}$$

consisting of two factors

$$F_1(\theta) = \frac{1}{e^{\kappa} - e^{-\kappa}} \cdot \left(\exp\{\kappa\} - \exp\{\kappa \cdot \cos(\theta)\}\right) \quad , \tag{27}$$

$$F_2(\varphi) = \frac{1}{2\,\pi} \cdot \varphi \quad . \tag{28}$$

Inverting $F_1(\theta)$ yields the individual quantile function

$$Q_1(p) = \cos^{-1}\left(\frac{1}{\kappa}\log\left(e^{\kappa} - p \cdot \left(e^{\kappa} - e^{-\kappa}\right)\right)\right) \quad , \tag{29}$$

$$= \cos^{-1}\left(1 + \frac{1}{\kappa} \cdot \mathrm{log1p}(p \cdot \mathrm{expm1}(-2\kappa))\right) \quad , \tag{30}$$

where (30) is a numerically optimized variant of (29), with the often available functions compensating for round-off error

$$\mathrm{log1p}(x) = \log(1 + x) \tag{31}$$

$$\mathrm{expm1}(x) = e^{x} - 1 \quad . \tag{32}$$

Note that similar transformations are used in stochastic sampling methods of the von Mises–Fisher transformation [34, Sec. II.A], [41, Sec. 3]. Together with the second individual quantile function, the inversion of (28),

$$Q_2(q) = 2\pi\, q \quad , \tag{33}$$

we obtain the complete quantile function

$$Q \;:\; \mathbb{R}^2 \to \mathbb{S}^2_{\mathrm{SC}} \tag{34}$$

$$Q \;:\; \begin{bmatrix}p \\ q\end{bmatrix} \to \begin{bmatrix}Q_1(p) \\ Q_2(q)\end{bmatrix} \quad , \tag{35}$$

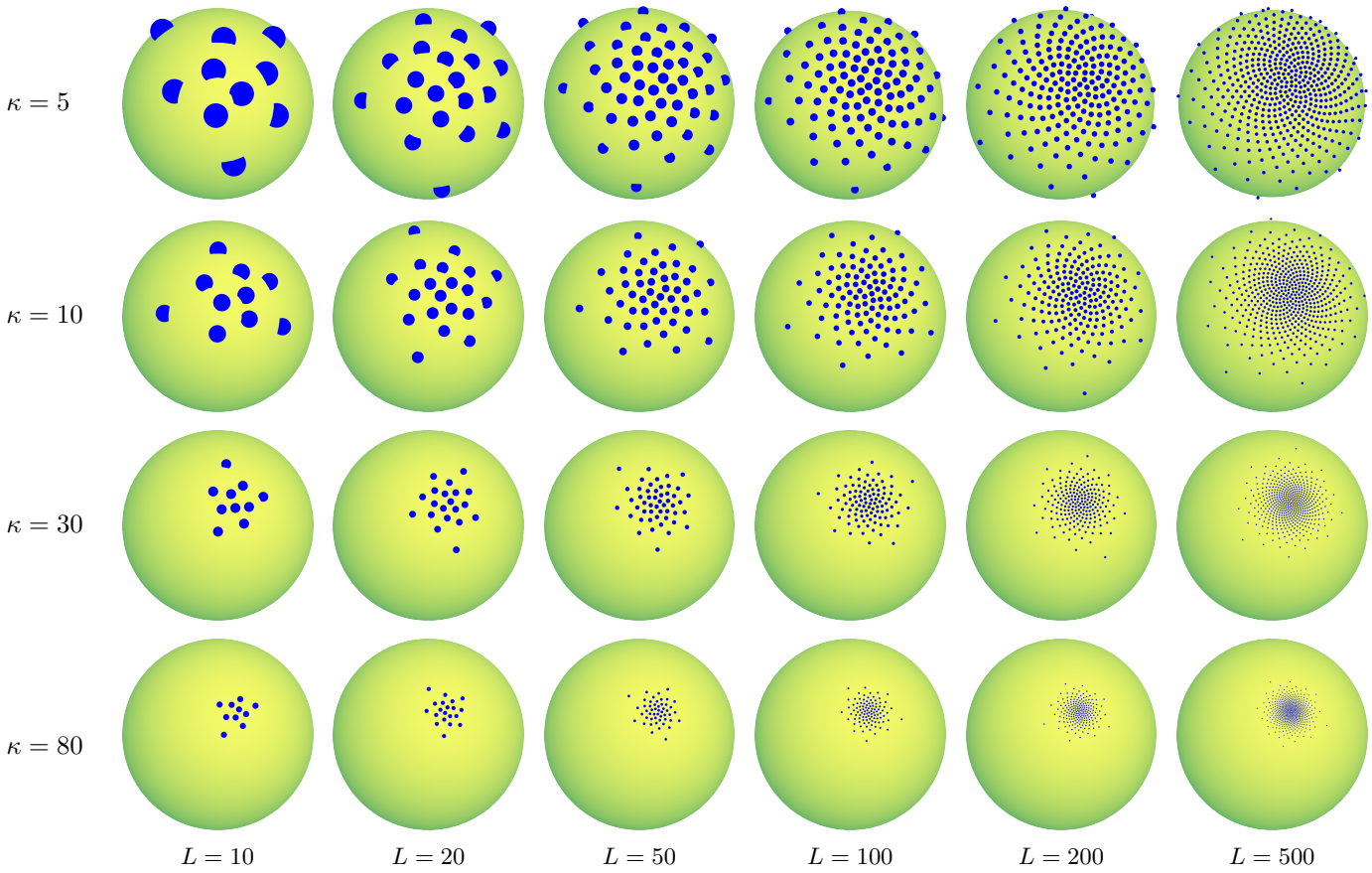

Fig. 6: Proposed von Mises–Fisher Samples (39) on the $\mathbb{S}^2$ sphere using Golden Kronecker samples (7) as uniform reference point set. Columns show different numbers of samples L, rows different concentration parameters κ.

that transforms uniform samples to von Mises–Fisher samples in spherical coordinates $[\theta, \varphi]^\top$. To obtain samples in Cartesian instead of spherical coordinates, we employ the mapping

$$\psi = \zeta \circ Q \colon \mathbb{R}^2 \to \mathbb{S}^2 \subset \mathbb{R}^3, \tag{36}$$

with coordinate transform ζ (21) and concatenation operator $\circ \colon f \circ g = f(g(\cdot))$. This transformation turns any two-dimensional low-discrepancy (or, trivially, random) sequence $\underline{x}_i^{\mathrm{u}}$ into von Mises–Fisher distributed samples $\underline{x}_i^f$

$$\underline{x}_i^f = \psi(\underline{x}_i^{\mathrm{u}}) \ , \tag{37}$$

$$\underline{x}_i^f \sim f(\underline{x}) \ . \tag{38}$$

In particular, choosing the centered Golden-Kronecker sequence (8) as the uniform reference point set, we obtain

$$\underline{x}_i^f = \begin{bmatrix} w \\ \sqrt{1-w^2} \cdot \cos\left(\frac{2\pi i}{\Phi}\right) \\ \sqrt{1-w^2} \cdot \sin\left(\frac{2\pi i}{\Phi}\right) \end{bmatrix} \ , \tag{39}$$

with

$$w = 1 + \frac{1}{\kappa} \cdot \mathrm{log1p}\left(\frac{2i-1}{2L} \cdot \mathrm{expm1}(-2\kappa)\right) \ . \tag{40}$$

See Figs. 1 and 6 for a visualization that is based on the Golden-Kronecker point set.

V. Mean Rotation

So far, we created samples with mean parameter $\underline{\mu} = \underline{e}_1$ and need a suitable transformation to obtain arbitrary mean values $\underline{\mu} \in \mathbb{S}^D$. Thus, we look for a rotation matrix $\mathbf{Q}$ with

$$\underline{\mu} = \mathbf{Q} \cdot \underline{e}_1 \ . \tag{41}$$

This sets the first column of $\mathbf{Q}$ to $\underline{\mu}$, and the other columns have to be chosen orthonormal to $\underline{\mu}$ and to each other, e.g., using the QR decomposition. See [34, Sec. II.C + Alg. 1] for more details.

VI. Evaluation

This section evaluates the proposed algorithm and compares it to existing methods using two quality measures. The first quality measure is the accuracy of κ. We draw von Mises–Fisher samples for $\kappa = 20$ (without any moment correction) with various sampling methods and for various numbers of samples. We then determine their κ using maximum likelihood estimation (MLE) [42] using the implementation in libDirectional [43] and compare it to the ground truth, $\kappa = 20$, respectively. The deviation is plotted over the number of samples, indicating the convergence properties (see Fig. 7a). Random samples were drawn according to [41], [44], using the implementation in libDirectional [43]. LCD sampling

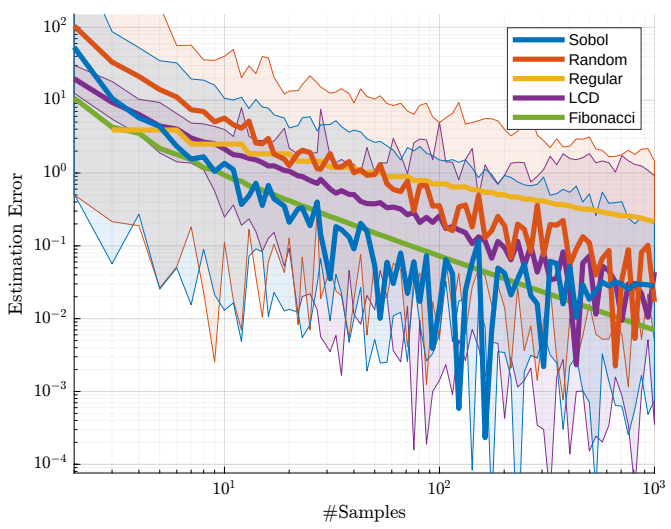

(a) κ Estimation

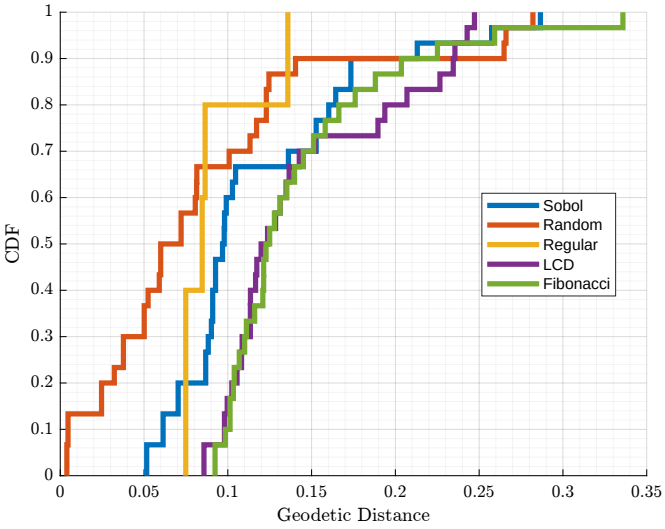

(b) Sample Spacing Statistics

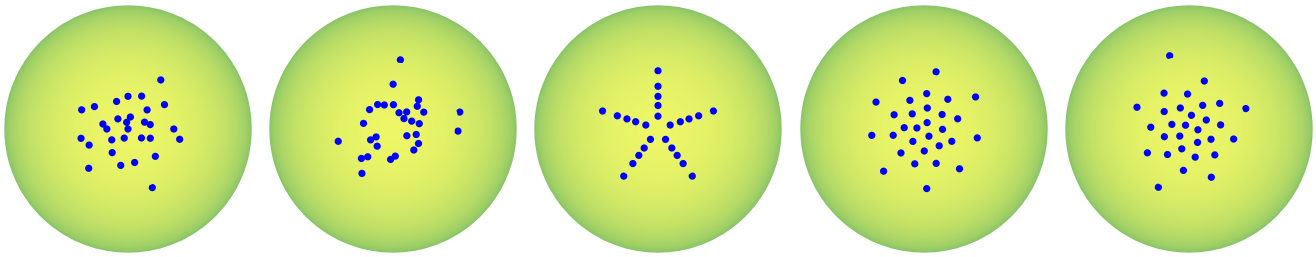

(c) Sobol (d) Random (e) Regular (f) LCD (g) Fibonacci

Fig. 7: (a) Evaluation by estimating the κ parameter for various numbers of samples, with 100 trials. (b) Cumulative empirical distribution of nearest neighbor distances for $L = 30$, $\kappa = 20$, see also bottom row for visualization of the samples.

was done by sample reduction [26] from the hundredfold number of random samples. The other methods were obtained by applying the proposed orthogonal inverse transform (30), (33) to uniform template samples, in particular, i) the Sobol set [45] with a random initial skip, ii) a centered regular Cartesian lattice as seen in Fig. 3b, resulting in orbit-planet-like arrangements, and iii) the centered Fibonacci-Kronecker lattice (8). When applicable, the range between the best and worst results out of 100 trials is indicated as a shaded area, and the mean as a thick line. See the bottom row of Fig. 7 for a visualization of the von Mises–Fisher samples from each of these methods for $L = 30$. The proposed method yields the best results in most cases, closely followed by LCD and Sobol-based samples.

As an alternative quality measure, we compare the empirical cumulative distribution (ECDF) of the geodetic distance $\cos^{-1}\left(\underline{x}_i^\top \cdot \underline{x}_j\right)$ between each sample $\underline{x}_i$ and its closest neighbor $\underline{x}_j$,

$$\min_{j \neq i} \left\{ \cos^{-1}\left(\underline{x}_i^\top \cdot \underline{x}_j\right) \right\} \tag{42}$$

(see Fig. 7b). LCD and Fibonacci methods generally achieve greater sample pair distance as they place samples more locally homogeneously.

Matlab source code is available on request and will eventually be published in [43], a MATLAB library for directional statistics and directional estimation, and on IEEE Code Ocean.

VII. Conclusion

We introduced a novel deterministic sampling method for the von Mises–Fisher distribution on the $\mathbb{S}^2$ sphere. It is based on the Fibonacci–Kronecker lattice as a uniform reference point set and an orthogonal inverse transform. Implementation is straightforward; the whole method boils down to a single formula (39). Other low-discrepancy point sets, such as the Sobol sequence, can also be used.

Regarding two measures, κ parameter estimation and local smoothness, the proposed samples achieve a higher quality than random samples and orbit-planet arrangements. Transformed Sobol samples, transformed Fibonacci samples (as proposed), and LCD samples share the winning places, depending on the specific application. LCD sampling is more complex to compute as it requires numerical optimization of the sample locations, so we achieve a promising tradeoff. Use cases of our method are scenarios where i) a higher number of samples is required than unscented sampling does provide, and ii) run time and computational complexity considerations make LCD sampling infeasible.

References

[1] J. Dick, F. Y. Kuo, and I. H. Sloan, "High-Dimensional Integration: The Quasi-Monte Carlo Way," *Acta Numerica*, vol. 22, pp. 133–288, 2013.

[2] S. Kucherenko and Y. Sytsko, "Application of Deterministic Low-Discrepancy Sequences in Global Optimization," *Computational Optimization and Applications*, vol. 30, no. 3, pp. 297–318, 2005.

[3] Á. González, "Measurement of Areas on a Sphere Using Fibonacci and Latitude–Longitude Lattices," *Mathematical Geosciences*, vol. 42, no. 1, p. 49, Nov. 2009.

[4] C. Godin, C. Golé, and S. Douady, "Phyllotaxis as Geometric Canalization During Plant Development," *Development*, vol. 147, no. 19, Oct. 2020.

[5] K. Mammasis and R. W. Stewart, "The FB5 Distribution and its Application in Wireless Communications," in *2008 International ITG Workshop on Smart Antennas*, 2008, pp. 375–381.

[6] G. Henry and D. Rodriguezs, "Robust Estimators in Partly Linear Regression Models on Riemannian Manifolds," *Communications in Statistics-Theory and Methods*, pp. 1–17, 2022.

[7] M. Fennel, A. Zea, and U. D. Hanebeck, "Optimization-Driven Design of a Kinesthetic Haptic Interface with Human-Like Capabilities," *IEEE Transactions on Haptics*, 2021.

[8] S. Calinon, "Gaussians on Riemannian Manifolds: Applications for Robot Learning and Adaptive Control," *IEEE Robotics & Automation Magazine*, vol. 27, no. 2, pp. 33–45, 2020.

[9] J. Wu, Z. Zhou, B. Gao, R. Li, Y. Cheng, and H. Fourati, "Fast Linear Quaternion Attitude Estimator Using Vector Observations," *IEEE Transactions on Automation Science and Engineering*, vol. 15, no. 1, pp. 307–319, 2018.

[10] P. Jäckel, "A Note on Multivariate Gauss-Hermite Quadrature," *London: ABN-Amro. Re*, 2005.

[11] E. A. Wan and R. Van Der Merwe, "The Unscented Kalman Filter for Nonlinear Estimation," in *Proceedings of the IEEE 2000 Adaptive Systems for Signal Processing, Communications, and Control Symposium (Cat. No. 00EX373)*. Ieee, 2000, pp. 153–158.

[12] M. F. Huber and U. D. Hanebeck, "Gaussian Filter based on Deterministic Sampling for High Quality Nonlinear Estimation," in *Proceedings of the 17th IFAC World Congress (IFAC 2008)*, vol. 17, no. 2, Seoul, Republic of Korea, Jul. 2008.

[13] D. Frisch and U. D. Hanebeck, "Deterministic Gaussian Sampling With Generalized Fibonacci Grids," in *Proceedings of the 24th International Conference on Information Fusion (Fusion 2021)*, Sun City, South Africa, Nov. 2021.

[14] U. D. Hanebeck, M. F. Huber, and V. Klumpp, "Dirac Mixture Approximation of Multivariate Gaussian Densities," in *Proceedings of the 2009 IEEE Conference on Decision and Control (CDC 2009)*, Shanghai, China, Dec. 2009.

[15] P. Leopardi, "A Partition of the Unit Sphere into Regions of Equal Area and Small Diameter," *ETNA. Electronic Transactions on Numerical Analysis [electronic only]*, vol. 25, pp. 309–327, 2006.

[16] F. Pfaff, K. Li, and U. D. Hanebeck, "The Spherical Grid Filter for Nonlinear Estimation on the Unit Sphere," in *Proceedings of the 1st Virtual IFAC World Congress (IFAC-V 2020)*, Jul. 2020.

[17] G. Kurz, I. Gilitschenski, and U. D. Hanebeck, "Unscented von Mises–Fisher Filtering," *IEEE Signal Processing Letters*, vol. 23, no. 4, pp. 463–467, Apr. 2016.

[18] K. Li, D. Frisch, B. Noack, and U. D. Hanebeck, "Geometry-Driven Deterministic Sampling for Nonlinear Bingham Filtering," in *Proceedings of the 2019 European Control Conference (ECC 2019)*, Naples, Italy, Jun. 2019.

[19] K. Li, F. Pfaff, and U. D. Hanebeck, "Progressive von Mises–Fisher Filtering Using Isotropic Sample Sets for Nonlinear Hyperspherical Estimation," *Sensors*, Apr. 2021.

[20] ——, "Hyperspherical Dirac Mixture Reapproximation," *arXiv preprint arXiv:2110.10411*, Oct. 2021.

[21] S. J. Julier and J. K. Uhlmann, "New Extension of the Kalman Filter to Nonlinear Systems," in *Signal Processing, Sensor Fusion, and Target Recognition VI*, vol. 3068. International Society for Optics and Photonics, Jul. 1997, pp. 182–193.

[22] K. Li, F. Pfaff, and U. D. Hanebeck, "Hyperspherical Deterministic Sampling Based on Riemannian Geometry for Improved Nonlinear Bingham Filtering," in *Proceedings of the 22nd International Conference on Information Fusion (Fusion 2019)*, Ottawa, Canada, Jul. 2019.

[23] ——, "Nonlinear von Mises–Fisher Filtering Based on Isotropic Deterministic Sampling," in *Proceedings of the 2020 IEEE International Conference on Multisensor Fusion and Integration for Intelligent Systems (MFI 2020)*, Virtual, Sep. 2020.

[24] D. Frisch and U. D. Hanebeck, "The Generalized Fibonacci Grid as Low-Discrepancy Point Set for Optimal Deterministic Gaussian Sampling," *Journal of Advances in Information Fusion*, vol. 18, no. 1, pp. 16–34, Jun. 2023.

[25] J. Steinbring, M. Pander, and U. D. Hanebeck, "The Smart Sampling Kalman Filter with Symmetric Samples," *Journal of Advances in Information Fusion*, vol. 11, no. 1, pp. 71–90, Jun. 2016.

[26] D. Frisch, K. Li, and U. D. Hanebeck, "Optimal Reduction of Dirac Mixture Densities on the 2-Sphere," in *Proceedings of the 1st Virtual IFAC World Congress (IFAC-V 2020)*, Jul. 2020.

[27] R. Fisher, "Dispersion on a Sphere," *Proceedings of the Royal Society of London. Series A, Mathematical and Physical Sciences*, vol. 217, no. 1130, pp. 295–305, 1953.

[28] P. E. J. Kanti V. Mardia, "Distributions on Spheres," in *Directional Statistics*, ser. Wiley Series in Probability and Statistics, jan 1999, pp. 159–192. [Online]. Available: https://doi.org/10.1002/9780470316979.ch9

[29] Á. F. García-Fernández, F. Tronarp, and S. Särkkä, "Gaussian Target Tracking With Direction-of-Arrival von Mises–Fisher Measurements," *IEEE Transactions on Signal Processing*, vol. 67, no. 11, pp. 2960–2972, 2019.

[30] I. Marković, F. Chaumette, and I. Petrović, "Moving Object Detection, Tracking and Following Using an Omnidirectional Camera on a Mobile Robot," in *2014 IEEE International Conference on Robotics and Automation (ICRA)*, 2014, pp. 5630–5635.

[31] F. Zhang, E. R. Hancock, C. Goodlett, and G. Gerig, "Probabilistic White Matter Fiber Tracking Using Particle Filtering and von Mises–Fisher Sampling," *Medical Image Analysis*, vol. 13, no. 1, pp. 5–18, 2009, includes Special Section on Medical Image Analysis on the 2006 Workshop Microscopic Image Analysis with Applications in Biology.

[32] A. Hinrichs and J. Oettershagen, "Optimal Point Sets for Quasi-Monte Carlo Integration of Bivariate Periodic Functions with Bounded Mixed Derivatives," in *Monte Carlo and Quasi-Monte Carlo Methods*, ser. Springer Proceedings in Mathematics & Statistics, R. Cools and D. Nuyens, Eds. Cham: Springer International Publishing, 2016, pp. 385–405.

[33] R. Marques, C. Bouville, K. Bouatouch, and J. Blat, "Extensible Spherical Fibonacci Grids," *IEEE Transactions on Visualization and Computer Graphics*, vol. 27, no. 4, pp. 2341–2354, 2021.

[34] G. Kurz and U. D. Hanebeck, "Stochastic Sampling of the Hyperspherical von Mises–Fisher Distribution Without Rejection Methods," in *Proceedings of the IEEE ISIF Workshop on Sensor Data Fusion: Trends, Solutions, Applications (SDF 2015)*, Bonn, Germany, Oct. 2015.

[35] B. D. Ripley, "Computer Generation of Random Variables: A Tutorial," *International Statistical Review / Revue Internationale de Statistique*, vol. 51, no. 3, pp. 301–319, 1983.

[36] D. Guo and X. Wang, "Quasi-Monte Carlo Filtering in Nonlinear Dynamic Systems," *IEEE Transactions on Signal Processing*, vol. 54, no. 6, pp. 2087–2098, 2006.

[37] A. Rahimnejad, S. A. Gadsden, and M. Al-Shabi, "Lattice Kalman Filters," *IEEE Signal Processing Letters*, vol. 28, pp. 1355–1359, 2021, conference Name: IEEE Signal Processing Letters.

[38] B. Keinert, M. Innmann, M. Sänger, and M. Stamminger, "Spherical Fibonacci Mapping," *ACM Transactions on Graphics (TOG)*, vol. 34, no. 6, pp. 1–7, 2015.

[39] D. D. Sokolov, "Spherical coordinates," Encyclopedia of Mathematics. [Online]. Available: http://encyclopediaofmath.org/index.php?title=Spherical_coordinates\&oldid=48774

[40] R. J. Purser, "Generalized Fibonacci Grids; A New Class of Structured, Smoothly Adaptive Multi-Dimensional Computational Lattices," pp. 1–38, May 2008. [Online]. Available: https://repository.library.noaa.gov/view/noaa/6956

[41] W. Jakob, "Numerically Stable Sampling of the von Mises-Fisher Distribution on S^2 (and Other Tricks)," *Interactive Geometry Lab, ETH Zürich, Tech. Rep*, p. 6, 2012.

[42] S. Sra, "A Short Note on Parameter Approximation for von Mises–Fisher Distributions: And a Fast Implementation of $Is(x)$," *Computational Statistics*, vol. 27, no. 1, pp. 177–190, 2012.

[43] G. Kurz, I. Gilitschenski, F. Pfaff, L. Drude, U. D. Hanebeck, R. Haeb-Umbach, and R. Y. Siegwart, "Directional Statistics and Filtering Using libDirectional," *Journal of Statistical Software*, vol. 89, no. 4, pp. 1–31, 2019.

[44] S. Jung, "Generating von Mises–Fisher Distribution on the Unit Sphere (S2)," *Tech. Rep.*, vol. 1, p. 2, 2009.

[45] I. M. Sobol', D. Asotsky, A. Kreinin, and S. Kucherenko, "Construction and Comparison of High-Dimensional Sobol' Generators," *Wilmott*, vol. 2011, no. 56, pp. 64–79, 2011.